



## Indentation of elastically anisotropic half-spaces by cones and parabolae of revolution

J. G. SWADENER†‡§ and G. M. PHARR†‡

† Metals and Ceramics Division, Oak Ridge National Laboratory, PO Box 2008, MS-6116, Oak Ridge, Tennessee 37831-6116, USA

‡ Department of Materials Science and Engineering, The University of Tennessee, Knoxville, Tennessee 37996-2200, USA

[Received 22 September 1999 and accepted in revised form 15 May 2000]

### ABSTRACT

Indentation of ceramic materials with smooth indenters such as parabolae of revolution and spheres can be conducted in the elastic regime to relatively high loads. Ceramic single crystals thus provide excellent calibration media for load- and depth-sensing indentation testing; however, they are generally anisotropic and a complete elastic analysis is cumbersome. This study presents a simplified procedure for the determination of the stiffness of contact for the indentation of an anisotropic half-space by a rigid frictionless parabola of revolution which, to first order, approximates spherical indentation. Using a similar approach, a new procedure is developed for analysing conical indentation of anisotropic elastic media. For both indenter shapes, the contact is found to be elliptical, and equations are determined for the size, shape and orientation of the ellipse and the indentation modulus.

### § 1. INTRODUCTION

Techniques for measuring the mechanical properties by load- and depth-sensing indentation are based on solutions to elastic contact problems (Pethica *et al.* 1983, Loubet *et al.* 1984, Doerner and Nix 1986, Oliver and Pharr 1992). Although solutions for isotropic media have been known for some time, the widespread use of elastically anisotropic materials in films, coatings, composites and microelectronics devices has recently focused attention on anisotropic elastic contact (Vlassak and Nix 1993, 1994). In addition, many hard ceramic materials can be indented entirely in the elastic regime and are therefore potentially useful as calibration materials for load- and depth-sensing indentation testing. However, these materials are generally highly anisotropic, and their use in calibration procedures requires an analysis which fully accounts for the anisotropy.

Using the Fourier transform technique, Willis (1966) determined the elastic solution for the indentation of an anisotropic half-space by a parabola of revolution. This solution takes the form of six nonlinear integral equations, which are difficult to apply in practice, because they must be solved simultaneously. Using the surface

---

§ Email: swadenerjg@ornl.gov.

Green's function for an anisotropic half-space (Barnett and Lothe 1975), Vlassak and Nix (1993, 1994) derived simplified expressions for the indentation parameters for the cases of flat punches of various shapes and for cases of indentation by a parabola of revolution with material symmetries that produce circular contact. The solution for a parabolic indenter on an elastic substrate was originally determined by Hertz (1882), and the solution for a transversely isotropic half-space was given by Elliott (1949).

The isotropic conical indentation problem was first solved by Love (1939) and more fully by Harding and Sneddon (1945). The first solution for transversely isotropic media was developed by Elliott (1949), but a solution for conical indentation of a general anisotropic half-space has not been presented.

In this study, we apply the surface Green's function determined by Barnett and Lothe (1975) to the indentation of an elastically anisotropic half-space by a parabola of revolution. To first order, this geometry also models spherical indentation. The indentation parameters are expressed in the form of contour integrals that can be evaluated directly in a manner more convenient than the procedure given by Willis.

The same technique is applied to conical indentation of an anisotropic half-space. For conical indentation, the projected area of contact is also shown to be elliptical. The solution determines expressions for the important indentation parameters.

To demonstrate the utility of these results, several examples of parabolic and conical indentation in elastically anisotropic materials are presented. The indentation modulus for sapphire is examined in some detail so as to provide results that can be used for the calibration of load- and depth-sensing testing using a sapphire substrate. Results are also presented for several cubic materials over a wide range of crystal orientations.

Extrapolation of these results to the case of an anisotropic indenter on an anisotropic substrate is possible for certain symmetries. Approximations for general cases of elastically anisotropic indenters and substrates are also discussed.

## §2. APPROACH

Similar methods are used to derive the important indentation parameters for contact by a parabola of revolution and by a cone, but the steps are in a different order. For the case of a parabola of revolution, many aspects of the solution are already known. Therefore, we start with some known results and from these develop additional formulae. For the case of a conical indenter, no previous solution exists. We use the semi-inverse method starting from assumptions about the pressure distribution that develops from conical contact. From the assumed pressure distribution, a solution is developed which is shown to justify the assumptions.

The analysis begins by relating the stiffness  $S$  of contact to the projected area  $A$  of contact. The stiffness of contact is an important parameter that is readily measured experimentally in indentation. Using the Fourier transform equations from Willis (1966) for indentation of an anisotropic half-space by a rigid and frictionless parabola of revolution, Vlassak and Nix (1993) showed that the contact stiffness for anisotropic materials can be written as

$$S = \frac{dP}{d\delta} = \frac{2}{\pi^{1/2}} MA^{1/2}, \quad (1)$$

where  $P$  is the applied load,  $\delta$  is the rigid-body displacement of the indenter relative to the half-space,  $A$  is the projected area of contact and  $M$  is the indentation modulus, which is a complicated function of the elastic moduli and, in general, is dependent on the shape of the indenter. A simplified formula for  $M$  will be presented herein for conical and parabolic indenters. For axisymmetric indenters and isotropic media, Pharr *et al.* (1992) have shown that equation (1) holds with  $M = E/(1 - \nu^2)$ , independent of the indenter geometry. For the special case of threefold or fourfold symmetry on the surface of the anisotropic half-space (which produces a circular projected area of contact), Vlassak and Nix (1993) have shown that  $M$  is the same for flat circular punches and parabolic indenters. For the general case, the projected area of contact is elliptical (Willis 1966), and  $M$  depends on the shape of the contact ellipse.

For indentation by a parabola of revolution, the relation between load and the displacement of the indenter, the pressure distribution and the projected area of contact are all known (Willis 1966). The surface displacements are derived from the surface Green's function (Barnett and Lothe 1975). Noting that the lateral surface displacements must be zero at the center of contact, a simplified procedure is developed to determine the orientation of the elliptical projected area of contact relative to the coordinate system used to define the stiffness tensor of the half-space. Once the orientation of the contact ellipse is known, the eccentricity of the ellipse is determined by again using the surface displacements. The surface displacements are also used to determine the indentation modulus  $M$ .

For a conical indenter, the initial assumptions are proposed and a solution is developed. In a manner similar to the previous case, the displacements of the surface are determined based on the assumed pressure distribution. The determination of the load–displacement relation, the indentation modulus and the orientation and eccentricity of the projected area of contact follow. The assumptions are verified by checking the consistency of the results with the boundary conditions.

### § 3. INDENTATION BY A PARABOLA OF REVOLUTION

For a rigid frictionless parabola of revolution initially resting on a general anisotropic half-space, the relation between  $P$  and  $\delta$  has been determined by Willis (1966) as

$$P = \frac{4M}{3\kappa^{1/2}} \delta^{3/2}, \quad (2)$$

where  $\kappa$  is the curvature at the tip of the indenter. The geometry of this problem is shown in figure 1. From equations (1) and (2), the contact stiffness for parabolic indentation is given by

$$S = \frac{dP}{d\delta} = \frac{2M}{\kappa^{1/2}} \delta^{1/2}. \quad (3)$$

For parabolic indenters on anisotropic media, Willis (1966) has shown that the projected area of contact is elliptical. Thus, the projected contact area is  $A = \pi a_1 a_2$ , where  $a_1$  and  $a_2$  are the semiaxes of the contact ellipse. Equating equations (1) and (3) and substituting for  $A$  relates the indenter displacement to the semiaxes of the contact ellipse as

$$\delta = a_1 a_2 \kappa. \quad (4)$$

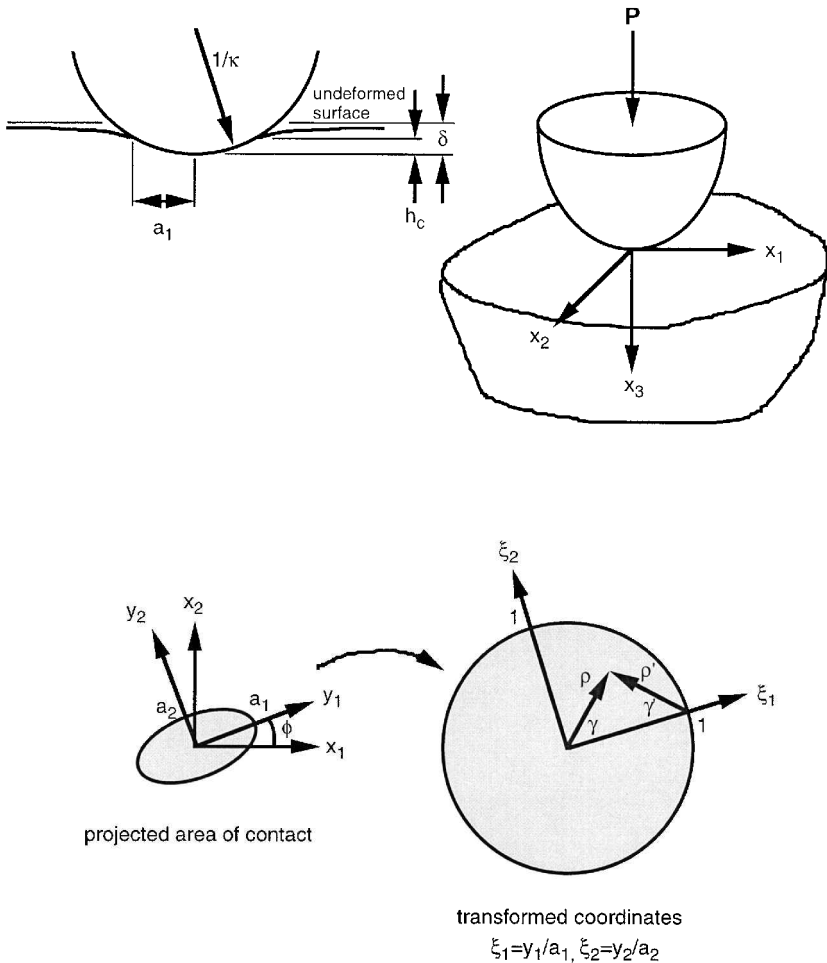


Figure 1. Geometry for indentation by a parabola of revolution.

For isotropic media, Doerner and Nix (1986) and Oliver and Pharr (1992) have shown that, even when plastic deformation occurs during indentation, the indentation modulus can still be determined experimentally from the elastic unloading behaviour. In order to use the Oliver–Pharr method, the contact depth must first be determined. In general terms, the contact depth can be written as (Oliver and Pharr 1992)

$$h_c = \delta - \varepsilon \frac{P}{S}, \tag{5}$$

where  $\varepsilon$  depends on the shape of the indenter. For parabolic indentation of isotropic media,  $\varepsilon = 0.75$  (Oliver and Pharr 1992). For parabolic indentation of anisotropic media, Vlassak and Nix (1993) have shown that the same value holds for the special case of threefold or fourfold symmetry on the surface of the half-space, which results in a circular projected contact area.

In general, the projected area of contact is elliptical, and the contact depth depends on the location along the edge of contact. On the major (or minor) elliptical

axis, the contact depth will be  $\kappa a_1^2/2$  while, on the minor (or major) axis, the contact depth will be  $\kappa a_2^2/2$ . Therefore, a logical choice for  $h_c$  is the mean value (averaged over the perimeter of contact), which can be written using equation (4) as

$$h_c = \frac{a_1 a_2}{2} \kappa = \frac{\delta}{2}. \tag{6}$$

Substituting equations (2), (4) and (6) into equation (5) gives  $\varepsilon = 0.75$  for elliptical contact, in agreement with previous results for circular contact and isotropic media.

### 3.1. Surface deformation

The surface Green's function for a half-space has been determined by Barnett and Lothe (1975) using the Stroh formalism. The displacements at the free surface ( $y_3 = 0$ ) in the  $x_i$  direction due to a unit force in the  $x_j$  direction are given by

$$u_{ij}(y_1, y_2, 0) = \frac{1}{2\pi|y|} \left( B_{ij}^{-1}(y) - \frac{1}{\pi} \int_0^\pi \frac{B_{ik}^{-1}(t) S_{kj}(t)}{\sin(\gamma - \gamma_0)} d\gamma \right), \tag{7}$$

where  $\mathbf{B}(t)$  and  $\mathbf{S}(t)$  are two of the Barnett–Lothe tensors computed on a plane whose normal lies in the  $y_1 y_2$  plane and makes an angle  $\gamma_0$  with the  $y_1$  axis and  $\gamma$  is also measured from the  $y_1$  axis. These Barnett–Lothe tensors are defined as (Barnett and Lothe 1975, Lothe and Barnett 1976)

$$\begin{aligned} \mathbf{B}(t) &= \frac{-1}{2\pi} \int_0^{2\pi} [(\mathbf{m}\mathbf{n})(\mathbf{m}\mathbf{n})^{-1}(\mathbf{n}\mathbf{m}) - (\mathbf{m}\mathbf{m})] d\varphi, \\ \mathbf{S}(t) &= \frac{-1}{2\pi} \int_0^{2\pi} [(\mathbf{n}\mathbf{n})^{-1}(\mathbf{n}\mathbf{m})] d\varphi, \end{aligned} \tag{8}$$

where the vectors  $(t, m, n)$  form an orthogonal right-hand system and  $\varphi$  is the angle between  $m$  and an arbitrary fixed datum in the plane normal to  $t$ . In the above expression, the second-order tensors  $(ab)$  are defined by  $(ab)_{jk} = a_i C_{ijkl} b_l$ , where  $C_{ijkl}$  are the components of the Cartesian stiffness tensor (the elastic moduli). Note that the tensors  $\mathbf{B}(t)$  and  $\mathbf{S}(t)$  do not depend on the magnitude of  $t$ .

Since  $\mathbf{B}$  is symmetric and positive definite and  $\mathbf{B}^{-1}\mathbf{S}$  is skew symmetric (Lothe and Barnett 1976), the surface displacements due to a unit load in the  $x_3$  direction reduce to (Vlassak and Nix 1993)

$$w_i(y) = \frac{1}{2\pi|y|} B_{ij}^{-1}(y) a_{3j}, \tag{9}$$

where  $a_{3j}$  are the direction cosines with the normal to the surface. Using this solution as a Green's function, the displacements of the surface for a pressure distribution  $p(y)$  over a surface  $S$  are given by

$$u(y) = \iint_S p(y') w(y - y') dy'. \tag{10}$$

For a rigid parabolic indenter in contact with an anisotropic elastic half-space, Willis (1966) has shown that the projected contact area is an ellipse and that the pressure distribution on the surface of the half-space is  $p(y_1, y_2) = p_0 [1 - (y_1/a_1)^2 - (y_2/a_2)^2]^{1/2}$ . Substituting this expression and equation (9) into equation (10) gives the surface displacements as

$$u_k(\mathbf{y}) = \frac{1}{2\pi} \iint_S \frac{p_0[1 - (y'_1/a_1)^2 - (y'_2/a_2)^2]^{1/2}}{|\mathbf{y} - \mathbf{y}'|} a_{kj} \mathbf{B}_{ij}^{-1}(\mathbf{y} - \mathbf{y}') a_{3j} d\mathbf{y}'. \quad (11)$$

The displacement of the indenter, which initially rests on the surface of the half-space, is equal to the surface displacement in the  $x_3$  direction at  $\mathbf{y} = \mathbf{0}$ , which is given by equation (11) as

$$\delta = \frac{1}{2\pi} \iint_S \frac{p_0[1 - (y'_1/a_1)^2 - (y'_2/a_2)^2]^{1/2}}{|\mathbf{y}'|} a_{3i} \mathbf{B}_{ij}^{-1}(\mathbf{y}') a_{3j} d\mathbf{y}'. \quad (12)$$

Using the coordinate transformation  $\rho \cos \gamma = y'_1/a_1$ ,  $\rho \sin \gamma = y'_2/a_2$ , this becomes

$$\begin{aligned} \delta &= \frac{p_0(a_1 a_2)^{1/2}}{2\pi} \int_0^{2\pi} \int_0^1 (1 - \rho^2)^{1/2} \frac{a_{3i} \mathbf{B}_{ij}^{-1}(\gamma) a_{3j}}{[(a_1/a_2) \cos^2 \gamma + (a_2/a_1) \sin^2 \gamma]^{1/2}} d\rho d\gamma \\ &= \frac{p_0(a_1 a_2)^{1/2}}{8} \int_0^{2\pi} \frac{a_{3i} \mathbf{B}_{ij}^{-1}(\gamma) a_{3j}}{[(a_1/a_2) \cos^2 \gamma + (a_2/a_1) \sin^2 \gamma]^{1/2}} d\gamma. \end{aligned} \quad (13)$$

Since the total applied force is  $\mathbf{P} = \int_S \mathbf{p}(\mathbf{y}) d\mathbf{y} = \frac{2}{3} \pi a_1 a_2 p_0$ , equation (13) can be written in the form

$$\delta = \frac{3\mathbf{P}}{16\pi(a_1 a_2)^{1/2}} \int_0^{2\pi} \frac{a_{3i} \mathbf{B}_{ij}^{-1}(\gamma) a_{3j}}{[(a_1/a_2) \cos^2 \gamma + (a_2/a_1) \sin^2 \gamma]^{1/2}} d\gamma. \quad (14)$$

In order to proceed further, the ratio  $a_1/a_2$  and the orientation  $\phi$  (see figure 1) of the ellipse relative to the chosen coordinate axes (which are implicit in the definition of the elastic moduli) must be determined.

### 3.2. Determination of $\phi$

If the surface possesses mirror symmetry, one axis of the contact ellipse must lie in the plane of symmetry. Otherwise, the orientation of the ellipse can be found by again using the surface displacements. At  $\mathbf{y} = \mathbf{0}$  the displacements in the direction of the elliptical axes must be zero owing to symmetry. Therefore, the displacement in any lateral direction must be zero at  $\mathbf{y} = \mathbf{0}$ . Thus, for the  $x_1$  direction, equation (11) gives

$$u_1(0) = 0 = \frac{1}{2\pi} \iint_S \frac{p_0[1 - (y'_1/a_1)^2 - (y'_2/a_2)^2]^{1/2}}{|\mathbf{y}'|} a_{1i} \mathbf{B}_{ij}^{-1}(\mathbf{y}') a_{3j} d\mathbf{y}'. \quad (15)$$

Using the same coordinate transformation as before, equation (15) can be reduced to

$$0 = \int_0^{2\pi} \frac{a_{1i} \mathbf{B}_{ij}^{-1}(\gamma) a_{3j}}{[(a_1/a_2) \cos^2 \gamma + (a_2/a_1) \sin^2 \gamma]^{1/2}} d\gamma. \quad (16)$$

When  $\phi$  is oriented correctly, equation (16) is insensitive to the choice of  $a_1/a_2$  owing to symmetry. The above equation depends on the orientation of  $\phi$  through the definition of  $\gamma$  (see figure 1). Therefore,  $\phi$  can be found by iteratively solving equation (16) for an arbitrary choice of  $a_1/a_2$ .

### 3.3. Determination of $a_1/a_2$

From the geometry of the problem, the deflection of the surface in the  $x_3$  direction at the end of semiaxis  $a_1$  is  $\delta - \kappa a_1^2/2$ . Using equation (4), this can be written as

$\delta(1 - a_1/2a_2)$ . Another expression for the surface deflection at  $\mathbf{y} = a_1\mathbf{y}_1$  can be found from equation (11). Equating these two expressions gives

$$\delta\left(1 - \frac{a_1}{2a_2}\right) = \frac{1}{2\pi} \iint_S \frac{p_0[1 - (y'_1/a_1)^2 - (y'_2/a_2)^2]^{1/2}}{[(a_1 - y'_1)^2 + (y'_2)^2]^{1/2}} a_{3i}B_{ij}^{-1}(a_1y_1 - \mathbf{y}')a_{3j} d\mathbf{y}'. \quad (17)$$

Transforming into polar coordinates about the point  $a_1\mathbf{y}_1$ ,  $\rho' \cos \gamma' = 1 - y'_1/a_1$ ,  $\rho' \sin \gamma' = y'_2/a_2$ , equation (17) becomes

$$\delta\left(1 - \frac{a_1}{2a_2}\right) = \frac{p_0(a_1a_2)^{1/2}}{2\pi} \int_{-\pi/2}^{\pi/2} \int_0^{2 \cos \gamma'} \frac{[2\rho' \cos \gamma' - (\rho')^2]^{1/2}}{[(a_1/a_2) \cos^2 \gamma' + (a_2/a_1) \sin^2 \gamma']^{1/2}} a_{3i}B_{ij}^{-1}(\gamma')a_{3j} d\rho' d\gamma'. \quad (18)$$

Performing the integration with respect to  $\rho'$  and substituting equation (13) for  $\delta$  gives the final form

$$\begin{aligned} \frac{1}{2} \left(1 - \frac{a_1}{2a_2}\right) \int_0^{2\pi} \frac{a_{3i}B_{ij}^{-1}(\gamma)a_{3j}}{[(a_1/a_2) \cos^2 \gamma + (a_2/a_1) \sin^2 \gamma]^{1/2}} d\gamma \\ = \int_{-\pi/2}^{\pi/2} \frac{(\cos^2 \gamma')a_{3i}B_{ij}^{-1}(\gamma')a_{3j}}{[(a_1/a_2) \cos^2 \gamma' + (a_2/a_1) \sin^2 \gamma']^{1/2}} d\gamma'. \end{aligned} \quad (19)$$

The ratio  $a_1/a_2$  can be found by iteratively solving the above equation. Thus the parabolic indentation problem is reduced to three integral equations, which are readily solvable one at a time in the order equations (16), (19) and (14).

### 3.4. Indentation modulus

From equations (1) and (2) and by differentiating equation (14) with respect to  $\delta$ , the contact stiffness for the indentation of an anisotropic half-space by a parabola of revolution can be written as

$$S = \frac{8\pi(\delta/\kappa)^{1/2}}{\int_0^{2\pi} \{a_{3i}B_{ij}^{-1}(\gamma)a_{3j}/[(a_1/a_2) \cos^2 \gamma + (a_2/a_1) \sin^2 \gamma]^{1/2}\}} d\gamma. \quad (20)$$

Thus, from equations (1), (4) and (20), the indentation modulus is derived as

$$M = \frac{4\pi}{\int_0^{2\pi} \{a_{3i}B_{ij}^{-1}(\gamma)a_{3j}/[(a_1/a_2) \cos^2 \gamma + (a_2/a_1) \sin^2 \gamma]^{1/2}\}} d\gamma. \quad (21)$$

For circular contact, equation (21) reduces to the result found by Vlassak and Nix (1993).

## §4. CONICAL INDENTATION

For indentation of an elastically anisotropic half-space by a rigid frictionless cone, the contact area and pressure distribution are not known *a priori*. Willis (1966) used the semi-inverse method for parabolic contact by assuming that the contact is elliptical and that the pressure distribution is similar to that for the case of an isotropic half-space. Hertz (1882) used the semi-inverse method for isotropic media, as did Love (1939) for a conical punch on an isotropic half-space. Using the

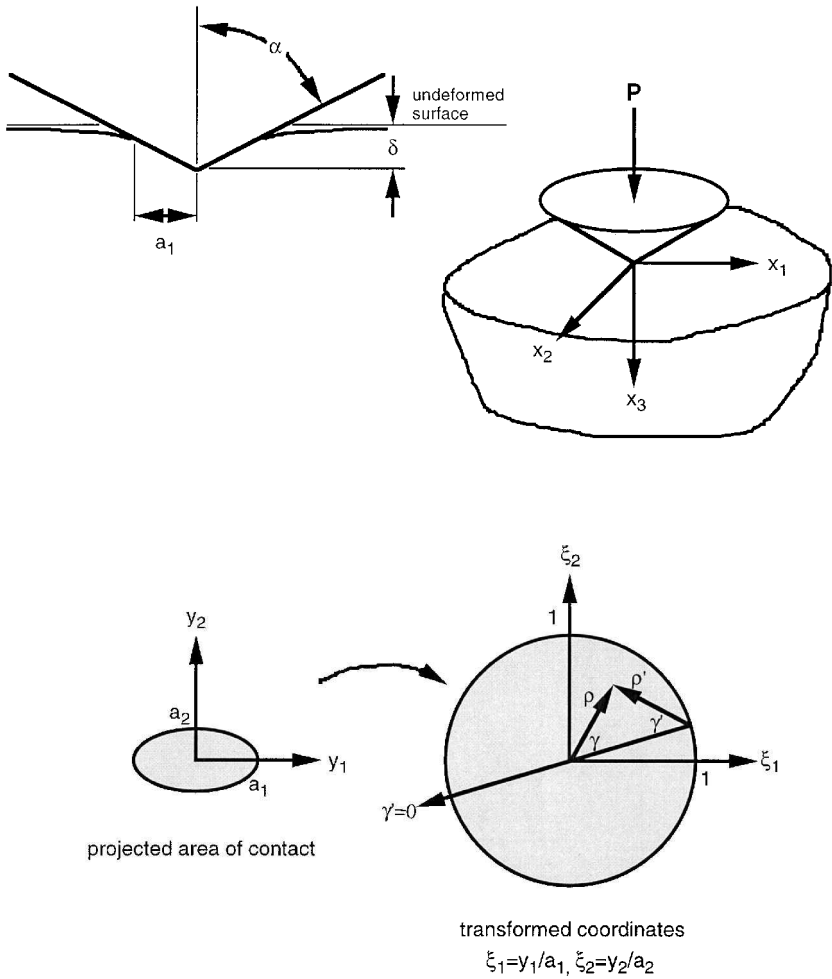


Figure 2. Geometry for conical indentation.

semi-inverse method for the current problem, the pressure distribution will be assumed to be a modification of the isotropic result acting over an elliptical region. The resulting displacements will be checked to verify that they match the prescribed boundary conditions. The geometry of this problem is shown in figure 2.

For conical indentation of an isotropic half-space, Love (1939) derived the pressure distribution as

$$p(r) = \frac{1}{2} M \cot \alpha \cosh^{-1} \left( \frac{a}{r} \right), \tag{22}$$

where  $\alpha$  is half the included angle of the cone,  $r$  is the radial coordinate and  $a$  is the contact radius. For a contact ellipse with semi-axes  $a_1$  and  $a_2$ , the assumed form of the pressure distribution will be

$$p(y_1, y_2) = p_0 \cosh^{-1} \left( \frac{1}{[(y_1/a_1)^2 + (y_2/a_2)^2]^{1/2}} \right), \tag{23}$$

where  $p_0$  is a constant that depends on the load. Later, the surface displacements will be calculated for this pressure distribution in order to verify the assumptions.

Again using the surface Green's function from Barnett and Lothe (1975), the surface displacements for the pressure distribution in equation (23) are

$$u_k(\mathbf{y}) = \frac{1}{2\pi} \iint_S \frac{p_0 \cosh^{-1} \{1/[(y'_1/a_1)^2 + (y'_2/a_2)^2]^{1/2}\}}{|\mathbf{y} - \mathbf{y}'|} a_{ki} B_{ij}^i(\mathbf{y} - \mathbf{y}') a_{3j} d\mathbf{y}'. \quad (24)$$

The displacement of the indenter, which initially rests on the surface of the half-space, is equal to the surface displacement in the  $x_3$  direction at  $\mathbf{y} = \mathbf{0}$ , which is given by equation (24) as

$$\delta = \frac{1}{2\pi} \iint_S \frac{p_0 \cosh^{-1} \{1/[(y'_1/a_1)^2 + (y'_2/a_2)^2]^{1/2}\}}{|\mathbf{y}'|} a_{3i} B_{ij}^{-1}(\mathbf{y}') a_{3j} d\mathbf{y}'. \quad (25)$$

Using the coordinate transformation  $\rho \cos \gamma = y'_1/a_1$ ,  $\rho \sin \gamma = y'_2/a_2$ , this becomes

$$\begin{aligned} \delta &= \frac{p_0(a_1 a_2)^{1/2}}{2\pi} \int_0^{2\pi} \int_0^1 \cosh^{-1} \left( \frac{1}{\rho} \right) \frac{a_{3i} B_{ij}^{-1}(\gamma) a_{3j}}{[(a_1/a_2) \cos^2 \gamma + (a_2/a_1) \sin^2 \gamma]^{1/2}} d\rho d\gamma \\ &= \frac{p_0(a_1 a_2)^{1/2}}{4} \int_0^{2\pi} \frac{a_{3i} B_{ij}^{-1}(\gamma) a_{3j}}{[(a_1/a_2) \cos^2 \gamma + (a_2/a_1) \sin^2 \gamma]^{1/2}} d\gamma. \end{aligned} \quad (26)$$

In terms of the total applied force  $P = \int_S p(\mathbf{y}) d\mathbf{y} = \pi a_1 a_2 p_0$ , equation (26) can be written as

$$\delta = \frac{P}{4\pi(a_1 a_2)^{1/2}} \int_0^{2\pi} \frac{a_{3i} B_{ij}^{-1}(\gamma) a_{3j}}{[(a_1/a_2) \cos^2 \gamma + (a_2/a_1) \sin^2 \gamma]^{1/2}} d\gamma. \quad (27)$$

#### 4.1. Indentation modulus

Since the projected area of contact is assumed to be elliptical, we can again make use of the contact stiffness relation (1). In order for conical indentation to be self-similar, the contact depth must be linearly related to the indenter displacement  $\delta$ . Therefore, the projected contact area  $A = \pi a_1 a_2$  must be proportional to  $\delta^2$ . Thus, the contact stiffness  $S$  is linear in  $\delta$  and, by integration of equation (1),

$$P = \frac{M}{\pi^{1/2}} \delta A^{1/2}. \quad (28)$$

By comparison with equation (27), the indentation modulus is

$$M = \frac{4\pi}{\int_0^{2\pi} \{a_{3i} B_{ij}^{-1}(\gamma) a_{3j} / [(a_1/a_2) \cos^2 \gamma + (a_2/a_1) \sin^2 \gamma]^{1/2}\} d\gamma}. \quad (29)$$

Note that this is the same expression as equation (21), which was derived for a parabolic indenter. However, the ratios  $a_1/a_2$  will in general be different for the two indenter shapes. (Note also that, using a similar procedure, the indentation modulus for a flat punch with an elliptical cross-section can be expressed in this form.)

For an isotropic half-space, the indenter displacement can be related to the radius  $a$  of contact as  $\delta = (\pi/2) a \cot \alpha$  (Love 1939, Harding and Sneddon 1945).

Elliott (1948) showed that this relation also holds for conical indentation normal to a transversely isotropic half-space. The anisotropic result must be reducible to the isotropic and transversely isotropic results which are independent of the elastic moduli. For self-similar contact, the displacement  $\delta$  must be linear in  $(a_1 a_2)^{1/2}$ . Therefore, the anisotropic relation can be written as

$$\delta = \frac{\pi}{2} (a_1 a_2)^{1/2} \cot \alpha. \tag{30}$$

The value of  $\varepsilon$  (equation (5)) will be derived on the basis again of the mean contact depth:

$$h_c = (a_1 a_2)^{1/2} \cot \alpha. \tag{31}$$

Using equations (3), (5) and (28), the contact depth can be written as

$$h_c = \delta - \varepsilon \frac{\delta}{2}. \tag{32}$$

Combining equations (30), (31) and (32) gives

$$\varepsilon = \frac{2}{\pi} (\pi - 2), \tag{33}$$

which is the same result as for the isotropic case (Oliver and Pharr 1992).

#### 4.2. Determination of $\phi$

The orientation of the contact ellipse is found in the same manner as for parabolic indentation. From equation (24), the equation for the lateral displacements at  $\mathbf{y} = \mathbf{0}$  in polar coordinates becomes

$$0 = \frac{p_0 (a_1 a_2)^{1/2}}{2\pi} \int_0^{2\pi} \int_0^1 \cosh^{-1} \left( \frac{1}{\rho} \right) \frac{a_{li} \mathbf{B}_{ij}^{-1}(\gamma) a_{3j}}{[(a_1/a_2) \cos^2 \gamma + (a_2/a_1) \sin^2 \gamma]^{1/2}} d\rho d\gamma. \tag{34}$$

After integration with respect to  $\rho$ , equation (34) can be reduced to the same expression as equation (16). For the correct value of  $\phi$ , equation (16) is not sensitive to the ratio  $a_1/a_2$ . Therefore, the orientations of the elliptical contact axes are the same for parabolic and conical indentation.

#### 4.3. Displacements at the edge of contact

Another coordinate transformation is utilized to simplify the expression for the surface displacements at the edge of the applied pressure distribution. First, the coordinate axes are aligned with the elliptical contact axes, which can be determined from equation (16) or from a line of mirror symmetry on the surface if one exists. The coordinate transformation  $\xi_1 = y_1/a_1$ ,  $\xi_2 = y_2/a_2$  then transforms the contact ellipse into a circle in the  $\xi$ -plane (see figure 2). In this coordinate system, the displacements can be written from equation (24) as

$$u_k(\xi) = \frac{p_0 (a_1 a_2)^{1/2}}{2\pi} \iint_{\sigma} \frac{\cosh^{-1} \{1/[(\xi_1')^2 + (\xi_2')^2]^{1/2}\}}{[(a_1/a_2)(\xi_1 - \xi_1')^2 + (a_2/a_1)(\xi_2 - \xi_2')^2]^{1/2}} a_{ki} \mathbf{B}_{ij}^{-1}(\xi - \xi') a_{3j} d\xi', \tag{35}$$

where  $\sigma$  is the unit circle in the  $\xi$  plane.

Next, a point on the edge of contact is chosen as the centre of a new coordinate system. The line  $\gamma' = 0$  runs from the chosen new origin through the origin in the  $\xi$

coordinate system, as shown in figure 2. The radial coordinate  $\rho'$  is the distance from the new origin, and  $\gamma'$  is the clockwise angle from the line  $\gamma' = 0$ . In this coordinate system, the surface displacements at the edge of contact become

$$u_k(\rho' = 0) = \frac{p_0(a_1 a_2)^{1/2}}{2\pi} \int_{-\pi/2}^{\pi/2} \int_0^{2 \cos \gamma'} \cosh^{-1} \left( \frac{1}{[(1 - \rho' \cos \gamma')^2 + (\rho' \sin \gamma')^2]^{1/2}} \right) \times \frac{a_{ki} B_{ij}^{-1}(\gamma') a_{3j}}{[(a_1/a_2) \cos^2 \gamma' + (a_2/a_1) \sin^2 \gamma']^{1/2}} d\rho' d\gamma'. \tag{36}$$

After integration with respect to  $\rho'$ , this reduces to

$$u_k(\rho' = 0) = \frac{p_0(a_1 a_2)^{1/2}}{2\pi} \int_{-\pi/2}^{\pi/2} (1 - |\sin \gamma'|) \frac{a_{ki} B_{ij}^{-1}(\gamma') a_{3j}}{[(a_1/a_2) \cos^2 \gamma' + (a_2/a_1) \sin^2 \gamma']^{1/2}} d\gamma'. \tag{37}$$

Note that the location around the edge of contact is implicit in the definition of  $\gamma'$ .

From equation (37), the displacement in the  $x_3$  direction at the edge of the pressure distribution is

$$u_3(\rho' = 0) = \frac{p_0(a_1 a_2)^{1/2}}{2\pi} \int_{-\pi/2}^{\pi/2} (1 - |\sin \gamma'|) \frac{a_{3i} B_{ij}^{-1}(\gamma') a_{3j}}{[(a_1/a_2) \cos^2 \gamma' + (a_2/a_1) \sin^2 \gamma']^{1/2}} d\gamma'. \tag{38}$$

These displacements, which result from the assumed pressure distribution (23), were found numerically to agree with the boundary conditions for conical indentation for several anisotropic cases. For a transversely isotropic half-space, equation (38) reduces to the known result (Elliot 1949, Hanson 1992).

Note that the solution is an approximation of the same order as the isotropic solution, that is the solution holds for angles  $\alpha$  close to  $90^\circ$ . Using finite-element analysis, Hay *et al.* (1999) have shown that, for  $\alpha = 70.3^\circ$ , errors of 6% occur in the indentation modulus of isotropic media with Poisson's ratio equal to 0.25. This is due to radial displacements of the surface. Accuracy similar to the isotropic case would be expected for the anisotropic case. For incompressible transversely isotropic media, the radial displacements are zero (Hanson 1992) and the solution is exact.

There is one more boundary condition which must be verified; outside the region of contact, the deformed surface must not penetrate the conical indenter. Verification of this boundary condition is presented in the appendix.

#### 4.4. Determination of $a_1/a_2$

From equation (30), the deflection of the surface in the  $x_3$  direction at the end of the contact ellipse semiaxis  $a_1$  is

$$\delta - a_1 \cot \alpha = \delta \left[ 1 - \frac{2}{\pi} \left( \frac{a_1}{a_2} \right)^{1/2} \right]. \tag{39}$$

Another expression for this deflection can be found from equation (38). Equating the two and substituting equation (26) for  $\delta$  give

$$\frac{1}{2} \left[ 1 - \frac{2}{\pi} \left( \frac{a_1}{a_2} \right)^{1/2} \right] \int_0^{2\pi} \frac{a_{3i} B_{ij}^{-1}(\gamma) a_{3j}}{[(a_1/a_2) \cos^2 \gamma + (a_2/a_1) \sin^2 \gamma]^{1/2}} d\gamma$$

$$= \int_{-\pi/2}^{\pi/2} (1 - |\sin \gamma'|) \frac{a_{3i} B_{ij}^{-1}(\gamma') a_{3j}}{[(a_1/a_2) \cos^2 \gamma' + (a_2/a_1) \sin^2 \gamma']^{1/2}} d\gamma'. \quad (40)$$

Once the orientation of the contact ellipse has been found from equation (16), the ratio  $a_1/a_2$  can be determined from equation (40) and the indentation modulus from equation (29).

## § 5. EXAMPLES

Two examples will be presented here to demonstrate the usefulness of this procedure. First, because it is potentially a useful calibration medium, both parabolic and conical indentation of single-crystal sapphire will be discussed. Second, parametric results for the indentation of cubic materials will be presented, because they represent a common class of anisotropic materials.

The procedures described above were used to determine the orientation of the elliptical projected area of contact, the ratio of the elliptical axes and the indentation modulus. Numerical integration was carried out in the same manner for all the integrals. The contour was discretized into segments of even length, and integration was performed by the third-order Newton–Cotes method. Convergence to within 0.01% was achieved using 120 segments.

### 5.1. Sapphire

Single-crystal sapphire is a readily obtainable material which is attractive for calibration procedures for several reasons. Sapphire can be loaded elastically to relatively high loads because of its high hardness. It can also be obtained in various sizes and crystal orientations with optically smooth surfaces. The current drawback to the use of sapphire as a calibration medium is that its indentation modulus is not known for parabolic and conical indentation. Sapphire possesses trigonal symmetry and thus has six independent elastic constants. Wachtman *et al.* (1960) determined these elastic constants as  $(C_{1111}, C_{1122}, C_{1133}, C_{1123}, C_{3333}, C_{2323}) = (496.72, 163.40, 110.73, -23.49, 497.98, 147.40)$  GPa, where the crystal  $a$  axis is oriented in the  $x_1$  direction, and the  $c$  axis in the  $x_3$  direction.

The indentation modulus of sapphire was determined for a range of orientations of the surface. For this example, the axis of indentation was normal to the surface, and the surface normal was aligned for a range of angles in one of three planes: the  $a$ – $c$  crystal plane or planes formed by the  $c$  axis and a line in the basal plane oriented at  $(\phi =) \pm 30^\circ$  from the  $a_1$  axis (figure 3). These latter two planes were shown by Wachtman *et al.* (1960) to have the greatest variation in elastic moduli. The orientation of the contact ellipse was verified by equation (16) to lie in the  $a$ – $c$  plane when the surface normal was in that plane. When the surface normal was in the  $\phi = 30^\circ$  or the  $\phi = -30^\circ$  plane, one of the elliptical axes was oriented in the direction of the projection in the plane of the surface of the  $a_2$  axis or the  $a_3$  axis respectively.

For spherical indentation, the ratio of the contact ellipse axes was determined from equation (19) for surface normals making an angle with the basal plane varying from  $0^\circ$  to  $90^\circ$ . The  $a_1/a_2$  values are shown in figure 4(a). For conical indentation, the  $a_1/a_2$  ratio was determined from equation (40) for the same range of surface normals. These results are shown in figure 4(b). As expected for trigonal symmetry,

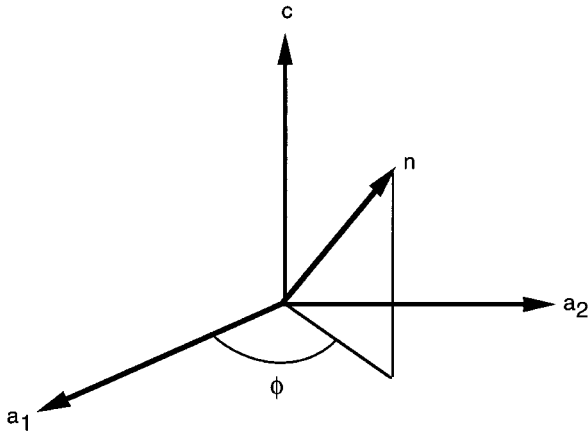


Figure 3. Plane containing the surface normal, which is oriented an angle  $\phi$  from the  $a_1$  axis.

the results for the three planes  $\phi = -30^\circ, 0^\circ, 30^\circ$  converge to  $a_1/a_2 = 1.0$  for indentation normal to the basal plane (parallel to the  $c$  axis;  $\phi = 90^\circ$ ) for both indenter geometries. Also, as expected, for indentation along a surface normal lying in the basal plane ( $\phi = 0^\circ$ ), the  $a_1/a_2$  ratio is independent of the orientation in the basal plane. As shown in figure 4, the eccentricity of the contact ellipse is larger for conical indentation than for parabolic indentation.

The indentation moduli for parabolic and conical indentation were determined using equations (20) and (29) and the  $a_1/a_2$  ratios shown in figure 4. The results for the surface orientation discussed above are plotted in figure 5 for both indenter geometries. For sapphire, the indentation modulus for conical indentation is within 0.1% of the value for parabolic indentation; so the results are not distinguished in figure 5. The indentation modulus of sapphire for conical and parabolic indentation was also found to be within 0.2% of its indentation modulus with a flat circular punch. For indentation with surface normals in other planes (other values of  $\phi$ ), the indentation modulus was calculated at selected points and found to lie at the expected locations in between the lines shown in figure 5. This regularity confirms the expectation based on the observations of Wachtman *et al.* (1960). Thus, the results shown in figure 5 represent the extreme values for single-crystal sapphire, and the indentation modulus for other surface orientations can be interpolated from these results.

### 5.2. Cubic materials

Crystals with cubic symmetry make up a broad class of materials. The three independent elastic moduli for this class can be normalized as two parameters: Poisson's ratio  $\nu = C_{1122}/(C_{111} + C_{1122})$  and the anisotropy factor  $F = 2C_{1212}/(C_{1111} - C_{1122})$ . Results are presented for selected values of  $F$  and  $\nu$  for indentation on a surface whose normal lies in the  $(1\bar{1}0)$  plane, which starts with the  $[110]$  direction, runs through the  $[111]$  direction and ends in the  $[001]$  direction. For indentation in this plane, mirror symmetry exists. Therefore, the direction of one of the contact ellipse's axes is the intersection of the  $(1\bar{1}0)$  plane with the surface plane. For parabolic indentation over a range of surface normal angles in this plane, the  $a_1/a_2$  ratio is plotted in figure 6 (a). For conical indentation,

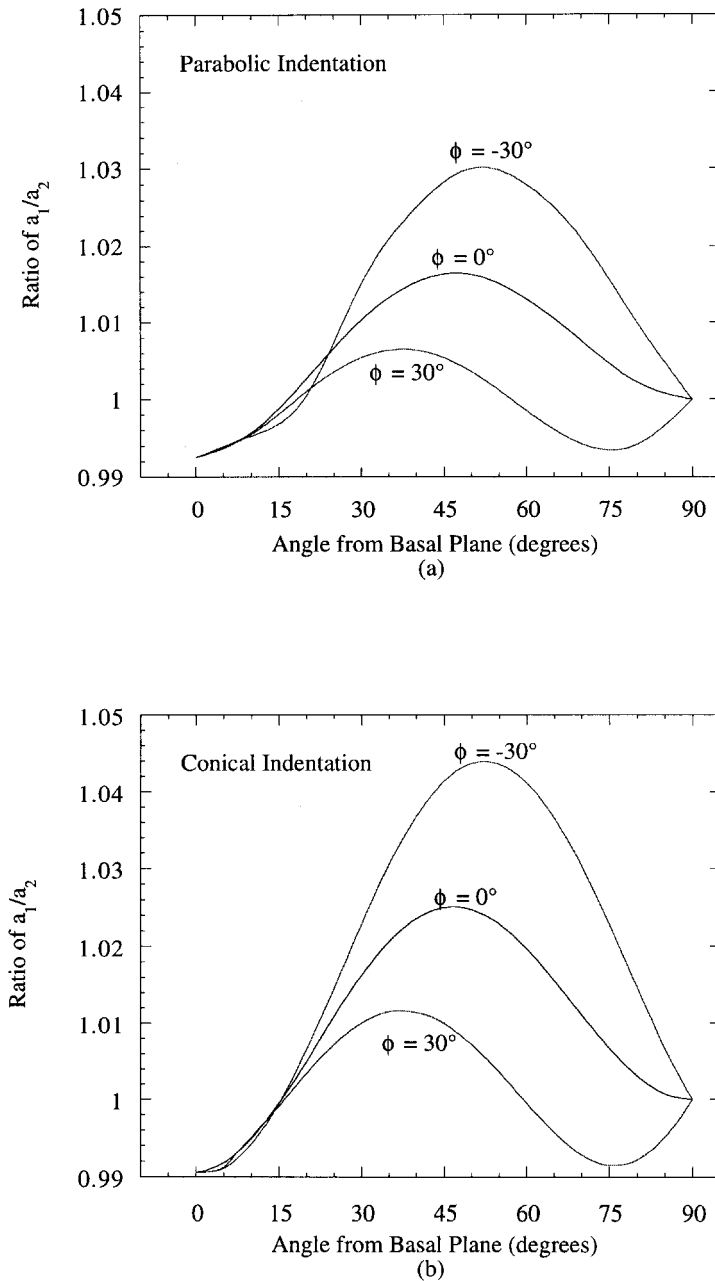


Figure 4. Variation on the ratio of the elliptical contact axes with surface orientation for (a) parabolic and (b) conical indentation of sapphire.

$a_1/a_2$  results for the same range of surface normals are shown in figure 6(b). As expected, circular contact occurs for surfaces normal to the [111] and [001] directions for all cases. Conical indentation causes greater eccentricity of the projected area of contact than parabolic indentation.

For the surface orientations discussed above, figure 7 shows the indentation modulus, normalized by the indentation modulus in the [001] direction. Only one

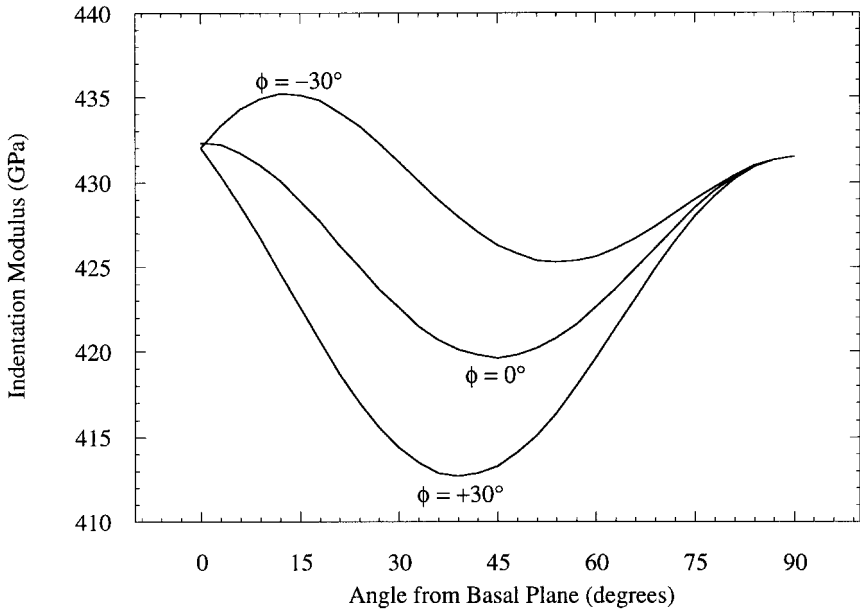


Figure 5. Variation in the indentation modulus with surface orientation for conical or parabolic indentation on a sapphire single-crystal half-space.

parabolic case ( $F = 5$ ;  $\nu = 0.1$ ) is plotted. For the other cases studied, the indentation moduli for the two indenter geometries were within 1% of each other. For all cases studied, the indentation modulus was found to be within 3% of the indentation modulus for a flat circular punch. For  $F = 1$ , figures 6 and 7 show that the isotropic result is recovered. For  $F > 1$ , the greatest indentation modulus is on the (111) surface.

### §6. DISCUSSION

The results presented here for contact between a rigid parabolic indenter on a half-space can be readily extended to the contact of two parabolae of revolution provided one of them is rigid. The method is the same as that used by Hertz (1882) for isotropic materials. The anisotropic extension is achieved by defining an effective curvature as  $\kappa = \kappa_1 + \kappa_2$ , where  $\kappa_1$  and  $\kappa_2$  are the curvatures of the two parabolae.

The problem of two anisotropic materials in contact is of sufficient importance to warrant special discussion. This problem frequently occurs in practice where indenters are generally composed of elastically anisotropic materials, for example diamond or sapphire. If both bodies possess threefold or fourfold symmetry on the surfaces in contact, then the projected areas of contact will be circular and the total compliance of contact will be the sum of the compliances for each body. Therefore, for circular contact, the effective indentation modulus is

$$M^* = \left( \frac{1}{M_1} + \frac{1}{M_2} \right)^{-1}, \quad (41)$$

where  $M_1$  and  $M_2$  are the indentation moduli of the two bodies. This result can be shown to hold for any indenter shape which gives circular contact.

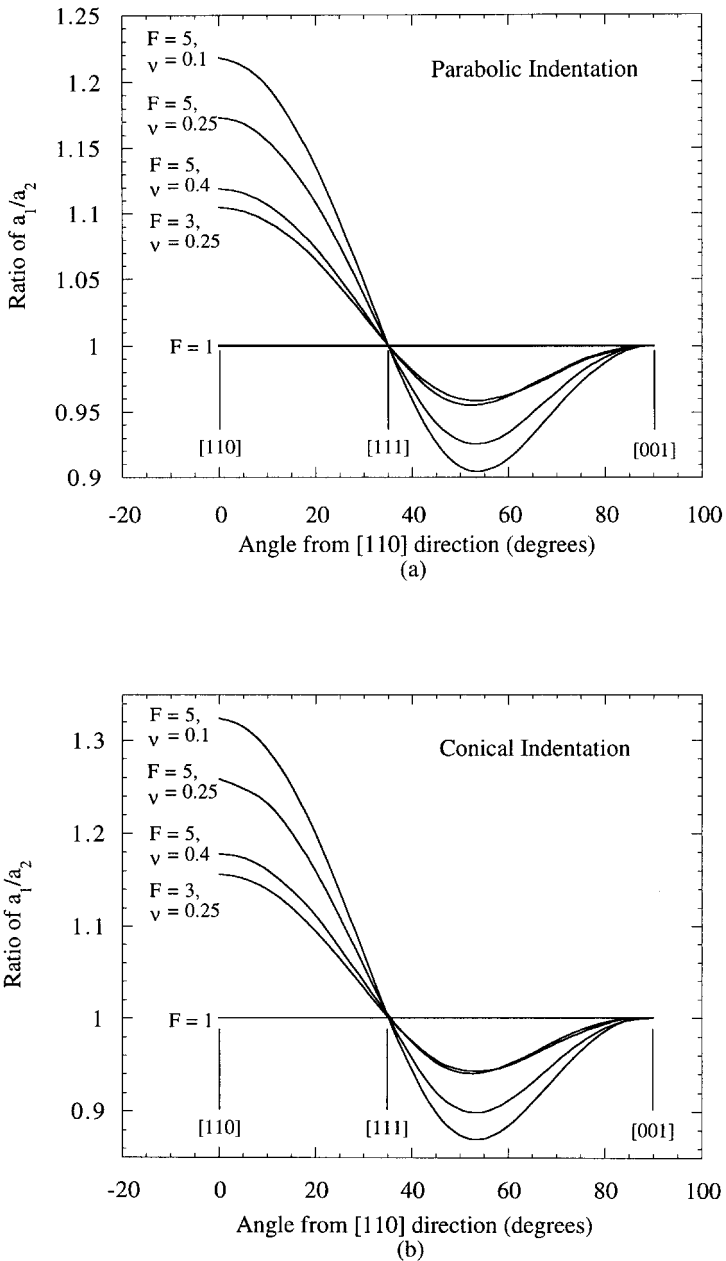


Figure 6. Variation in the ratio of the elliptical contact axes with surface orientation for (a) parabolic and (b) conical indentation of cubic single crystals.

For cases where contact is not circular, the exact shape and orientation of the projected area of contact must be calculated numerically. However, for a broad range of anisotropic materials, it has been shown that the indentation modulus for elliptical contact is within 3% of the indentation modulus for circular contact. Therefore, if the indentation moduli for parabolic or conical indentation are close

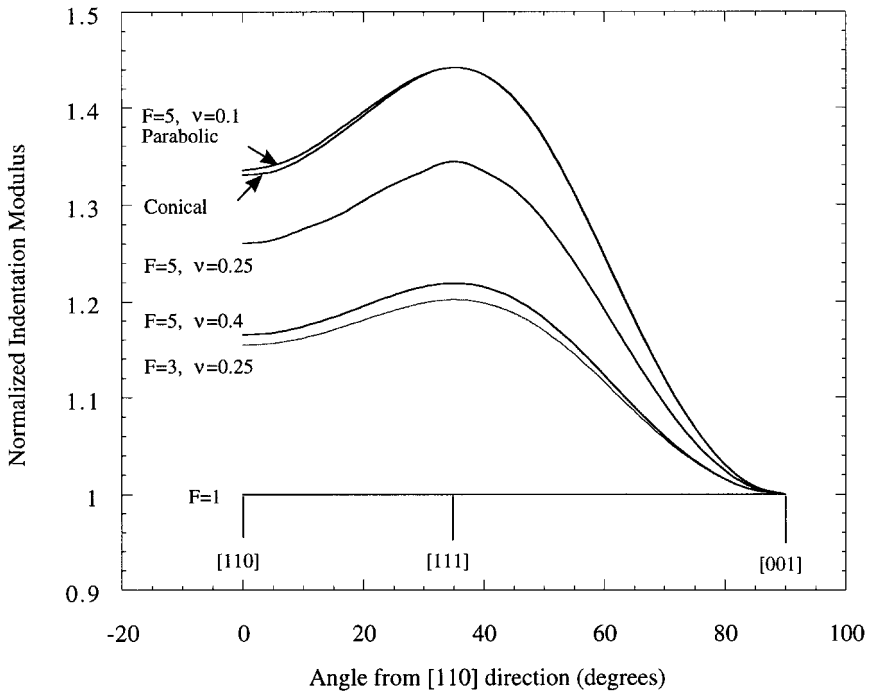


Figure 7. Variation with surface orientation in the indentation modulus normalized by the indentation modulus in the [100] direction for conical and parabolic indentation of cubic single crystals.

to the values for a circular punch, it is anticipated that equation (41) will be approximately correct for elliptical contact.

#### § 7. SUMMARY

The indentation of an anisotropic half-space by a rigid frictionless cone was shown to produce an elliptical projected area of contact similar to the case for indentation with a rigid frictionless parabola of revolution. The case of the parabolic indenter was determined previously (Willis 1960), but the conical case is new.

Contour integral formulas were presented for the orientation and eccentricity of the elliptical projected area of contact for each indenter geometry. The indentation moduli for both geometries were found to be given by the same expression. However, the actual indentation moduli were shown to be different owing to the different contact areas for the two indenter geometries.

The indentation modulus of single-crystal sapphire was determined for the complete range of surface orientations. The results can be used for many indentation calibration procedures. For cubic materials, the indentation modulus was determined for a wide range of surface orientations and material properties.

#### ACKNOWLEDGEMENTS

Research at the Oak Ridge National Laboratory SHaRE user facility was sponsored by the Division of Materials Sciences, US Department of Energy, under contract DE-AC05-96OR22464 with Lockheed Martin Energy Research

Corporation. The authors wish to thank Dr Ian Anderson of Oak Ridge National Laboratory for his careful reading of this paper and his helpful suggestions.

APPENDIX

The boundary condition that requires no interpretation of the conical indenter and the half-space can be formulated in terms of the coordinates  $\xi_1 = y_1/a_1$ ,  $\xi_2 = y_2/a_2$ , as

$$\delta - u_3(\xi) \leq |\xi| \cot \alpha, \quad |\xi| \geq 1. \tag{A 1}$$

For large values of  $|\xi|$ ,  $u_3(\xi) \rightarrow 0$  and equation (A 1) is satisfied. In order to verify equation (A 1) in the neighbourhood near  $|\xi| = 1$ , it is sufficient to show that

$$-\frac{\partial u_3(\xi)}{\partial |\xi|} \leq \cot \alpha. \tag{A 2}$$

In the neighbourhood of  $(\xi_1, \xi_2) = (1, 0)$ , the expression for  $u_3(1 + \varepsilon, 0)$  from equation (35) can be written in terms of the coordinates  $\rho \cos \gamma = 1 - \xi_1$  and  $\rho \sin \gamma = \xi_2$  as

$$\begin{aligned} u_3(1 + \varepsilon, 0) &= \frac{p_0(a_1/a_2)^{1/2}}{2\pi} \int_{-\pi/2}^{\pi/2} \int_0^{2 \cos \gamma} \\ &\times \cosh^{-1} \left( \frac{1}{[(1 - \rho \cos \gamma)^2 + (\rho \sin \gamma)^2]^{1/2}} \right) \\ &\times \frac{a_{3i} B_{ij}^{-1}(\xi - \xi') a_{3j}}{[(a_1/a_2)(\rho' \cos \gamma' + \varepsilon)^2 + (a_2/a_1)(\rho' \sin \gamma')^2]^{1/2}} \rho d\rho d\gamma, \end{aligned} \tag{A 3}$$

where  $\xi'_1 = \xi_1 + \varepsilon$ ,  $\xi'_2 = \xi_2$ ,  $\rho' \cos \gamma' = \rho \cos \gamma + \varepsilon$  and  $\rho' \sin \gamma' = \rho \sin \gamma$ . Then, from equation (A 3),

$$\begin{aligned} -\frac{\partial u_3(\xi)}{\partial |\xi|} \Big|_{(1,0)} &= -\lim_{\varepsilon \rightarrow 0^+} \left( \frac{\partial u_3}{\partial \varepsilon} \right) \\ &= \lim_{\varepsilon \rightarrow 0^+} \left[ \frac{p_0(a_1 a_2)^{1/2}}{2\pi} \int_{-\pi/2}^{\pi/2} \int_0^{2 \cos \gamma} \right. \\ &\times \cosh^{-1} \left( \frac{1}{[(1 - \rho \cos \gamma)^2 + (\rho \sin \gamma)^2]^{1/2}} \right) \\ &\times \frac{(a_1/a_2)(\rho' \cos \gamma' + \varepsilon) a_{3i} B_{ij}^{-1}(\xi - \xi') a_{3j}}{[(a_1/a_2)(\rho' \cos \gamma' + \varepsilon)^2 + (a_2/a_1)(\rho' \sin \gamma')^2]^{3/2}} \rho d\rho d\gamma \Big]. \end{aligned} \tag{A 4}$$

Since the integral in equation (A 4) converges as  $\varepsilon \rightarrow 0^+$ , the limit may be taken inside the integral which gives:

$$\begin{aligned}
 -\frac{\partial u_3(\xi)}{\partial|\xi|} \Big|_{(1,0)} &= \frac{p_0(a_1 a_2)^{1/2}}{2\pi} \int_{-\pi/2}^{\pi/2} \int_0^{2 \cos \gamma} \cosh^{-1} \left( \frac{1}{[(1 - \rho \cos \gamma)^2 + (\rho \sin \gamma)^2]^{1/2}} \right) \\
 &\quad \times \frac{(a_1/a_2) (\cos \gamma) a_{3i} B_{ij}^{-1}(\gamma) a_{3j}}{[(a_1/a_2) \cos^2 \gamma + (a_2/a_1) \sin^2 \gamma]^{3/2}} \frac{1}{\rho} d\rho d\gamma, \tag{A 5}
 \end{aligned}$$

where the relations  $\rho \rightarrow \rho'$  and  $\gamma \rightarrow \gamma'$  as  $\varepsilon \rightarrow 0^+$  have been utilized.

The integration with respect to  $\rho$  in equation (A 5) is accomplished by using a Taylor series expansion about 1:

$$\begin{aligned}
 I_1 &= \int_0^{2 \cos \gamma} \cosh^{-1} \left( \frac{1}{[(1 - \rho \cos \gamma)^2 + (\rho \sin \gamma)^2]^{1/2}} \right) \frac{1}{\rho} d\rho \\
 &= \int_0^{2 \cos \gamma} \sum_{n=1}^{\infty} \frac{-1^{n+1} (2 \cos \gamma - \rho)^{n/2}}{n} \rho^{n/2-1} d\rho \\
 &\quad - \frac{1}{2} \int_0^{2 \cos \gamma} \sum_{n=1}^{\infty} \frac{-1^{n+1} (\rho - 2 \cos \gamma)^n}{n} \rho^{n-1} d\rho. \tag{A 6}
 \end{aligned}$$

The above integration is simplified by using the change of variable  $\rho = 2 \cos \gamma \sin^2 \theta$ . Upon integration, equation (A 6) becomes

$$I_1 = \sum_{n=1}^{\infty} \frac{-1^{n+1} \Gamma(n/2 + 1) \Gamma(n/2)}{n \Gamma(n + 1)} (2 \cos \gamma)^n - \sum_{n=1}^{\infty} \frac{-1^{n+1} \Gamma(n + 1) \Gamma(n)}{2n \Gamma(2n + 1)} (2 \cos \gamma)^{2n}. \tag{A 7}$$

Now equation (A 5) can be written as

$$-\frac{\partial u_3(\xi)}{\partial|\xi|} \Big|_{(1,0)} \leq \frac{p_0(a_1 a_2)^{1/2}}{2\pi} \int_{-\pi/2}^{\pi/2} I_1 \frac{a_{3i} B_{ij}^{-1}(\gamma) a_{3j}}{[(a_1/a_2) \cos^2 \gamma + (a_2/a_1) \sin^2 \gamma]^{1/2}} d\gamma. \tag{A 8}$$

Using equation (26), equation (A 8) can be written in terms of  $\delta$  as

$$\begin{aligned}
 -\frac{\partial u_3(\xi)}{\partial|\xi|} \Big|_{(1,0)} &\leq \\
 &\leq \frac{2\delta}{\pi} \frac{\int_{-\pi/2}^{\pi/2} I_1 \{a_{3i} B_{ij}^{-1}(\gamma) a_{3j} / [(a_1/a_2) \cos^2 \gamma + (a_2/a_1) \sin^2 \gamma]^{1/2}\} d\gamma}{\int_0^{2\pi} \{a_{3i} B_{ij}^{-1}(\gamma) a_{3j} / [(a_1/a_2) \cos^2 \gamma + (a_2/a_1) \sin^2 \gamma]^{1/2}\} d\gamma} \\
 &= \frac{2\delta}{\pi} f, \tag{A 9}
 \end{aligned}$$

where  $f$  is a constant. For the range of material properties presented in § 4, the value of  $f$  was calculated numerically and found to be between 0.97 and 1.0.

In the  $\xi$ -coordinate system,  $a_1 a_2 = 1$ , and equation (30) becomes  $\delta = \pi \cos(\alpha/2)$ . Substituting this expression for  $\delta$  into equation (A 9) gives the final result

$$-\frac{\partial u_3(\xi)}{\partial|\xi|} \Big|_{(1,0)} \leq f \cot \alpha. \tag{A 10}$$

For  $(\xi_1, \xi_2) = (0, 1 + \varepsilon) = (\rho \cos \gamma, \rho \sin \gamma + \varepsilon)$ , the factor  $(a_1/a_2) \cos \gamma$  in equation (A 5) is replaced by the factor  $(a_2/a_1) \sin \gamma$ , and the same equation (A 8) can be derived. Therefore, evaluation of the slope of the surface at any location around the edge of contact will yield equation (A 10), and the boundary condition is found to be satisfied around the periphery of contact for a broad range of material properties.

## REFERENCES

- BARNETT, D. M., and LOTHER, J., 1975, *Phys. Norvegica*, **8**, 13.  
 DOERNER, M. F., and NIX, W. D., 1986, *J. Mater. Res.*, **1**, 601.  
 ELLIOTT, H. A. 1949, *Proc. Camb. Phil. soc.*, **45**, 621.  
 HANSON, M. T., 1992, *J. appl. Mech.*, **59**, S123.  
 HARDING, J. W., and SNEDDON, I. N., 1945, *Proc. Camb. Phil. Soc.*, **41**, 16.  
 HAY, J. C., BOLSHAKOV, A., and PHARR, G. M., 1999, *J. Mater. Res.*, **14**, 2296.  
 HERTZ, H., 1882, *J. reine angew. Math.*, **92**, 156.  
 LOTHE, J., and BARNETT, D. M., 1976, *J. appl. Phys.*, **47**, 428.  
 LOUBET, J. L., GEORGES, J. M., MARCHESINI, O., and MEILLE, G., 1984, *J. Tribol.*, **106**, 43.  
 LOVE, A. E. H., 1939, *Q. J. appl. Math.*, **10**, 161.  
 OLIVER, W. C., and PHARR, G. M., 1992, *J. Mater. Res.*, **7**, 1564.  
 PETHICA, J. B., HUTCHINGS, R., and OLIVER, W. C., 1983, *Phil. Mag. A*, **48**, 593.  
 PHARR, G. M., OLIVER, W. C., and BROTZEN, F. R., 1992, *J. Mater. Res.* **7**, 613.  
 VLASSAK, J. J., and NIX, W. D., 1993, *Phil. Mag. A*, **67**, 1045; 1994, *J. Mech. Phys. Solids*, **42**, 1223.  
 WACHTMAN, J. B., Jr., TEFFT, W. E., LAM, D. G., Jr., and STINCHFIELD, R. P., 1960, *J. Res. Natl Bureau of Standards*, **64A**, 213.  
 WILLIS, J. R., 1966, *J. Mech. Phys. Solids*, **14**, 163.